Available online at www.sciencedirect.com
SCIENCE DIRECT®
Journal of the European Ceramic Society 25 (2005) 969–977
www.elsevier.com/locate/jeurceramsoc

Modulus and hardness evaluation of polycrystalline superconductors by dynamic microindentation technique

Orhan Uzun [a,*], Uğur Kölemen [a], Selahattin Çelebi [b], Nusret Güçlü [a]

[a] *Department of Physics, Faculty of Science and Arts, Gaziosmanpaşa University, 60240 Tokat, Turkey*
[b] *Department of Physics, Faculty of Science and Arts, Karadeniz Technical University, 61080 Trabzon, Turkey*

Received 14 January 2004; received in revised form 10 March 2004; accepted 24 March 2004
Available online 20 June 2004

Abstract

In this study, depth-sensing Vickers indentation tests were conducted on polycrystalline superconductors under different peak load (0.49, 0.73, 0.98, and 1.22 N). The load (P)–penetration depth (h) curves were analyzed in order to evaluate the mechanical characteristics such as microhardness and elastic modulus. It was found that both of these characteristics exhibited significant peak load dependence which suggested a need for calculation of the load-independent hardness and modulus. The load independent hardness (0.88, 0.95, and 1.12 GPa) and modulus (1.98, 3.13, and 3.33 GPa) values were then calculated for YBCO, YBCO + 0.5% ZnO, and YBCO + 1% ZnO, respectively.

Keywords: Indentation; Hardness; Elastic modulus; Superconductors; YBCO

1. Introduction

Practical applications of $YBa_2Cu_3O_x$ (YBCO; Y-123), $Bi_2Sr_2Ca_1Cu_2O_8$ (BSCCO; Bi-2212), and $Bi_2Sr_2Ca_2Cu_3O_{10}$ (BSCCO; Bi-2223) superconducting compounds are often limited by their poor mechanical performance, i.e. extremely low ductility and elevated brittleness. For the successful application of high-temperature oxide superconductors ceramic (poly or single crystals) materials such as Y-123 ($T = 92$ K), Bi-2212 ($T = 85$ K), and Bi-2223 ($T = 110$ K), the information on its physical properties is essential.

On the other hand, the mechanical properties such as hardness, Young's modulus, fracture toughness, ductility, etc. are as important as the critical temperature, the critical current density, and the critical magnetic field for industrial applications of high-temperature oxide superconductors. As the superconducting material is drawn, rolled, or pressed, it may be subjected to several mechanical deformation processes. Optimization of these processes, minimization of the generation of deleterious microcracks, and achievement of structural reliability for applications require substantial knowledge of the mechanical behaviour of the ceramic superconductors.

Regarding mechanical properties, hardness testing provides useful information on the strength and deformative characteristics of the materials (elastic modulus, elastic recovery hardness, etc.).[1] Hardness is a mechanical parameter which is strongly related to the structure and composition of solids. Hence, microhardness is not only a mechanical characteristic routinely measured but it has also been developed as an investigation method of structural parameters in recent years. Therefore, hardness experiments have become more and more important to characterize a material [2–4].

The characteristic ability of a material to resist penetration of an indenter allows evaluation of a parameter that we know hardness. The indentation hardness of materials is measured in several ways by forcing an indenter having specific geometry (ball, cone, and pyramid) into the specimens' surface.[5]

The conventional microhardness value can be determined from the optical measurement of the residual impression left behind upon load release. In recent decades, the development of depth-sensing indentation equipment has allowed the easy and reliable determination of two of the most commonly measured mechanical properties of materials, the hardness and Young's modulus.[6] The depth-sensing (or dynamic) microindentation method offers great advantages over the

* Corresponding author. Tel.: +90 356 252 15 96; fax: +90 356 252 15 85.
E-mail address: ouzun@gop.edu.tr (O. Uzun).

0955-2219/$ – see front matter © 2004 Elsevier Ltd. All rights reserved.
doi:10.1016/j.jeurceramsoc.2004.03.031

conventional Vickers microhardness testing in two aspects. Firstly, apart from microhardness (or microstrength), the method can also provide well-defined mechanical parameters such as elastic modulus of the interfacial zone. Secondly, as load and depth of an indentation are continuously monitored, optical observation and measurement of diagonal length of the indent/impression, which can be difficult and subjected to inaccuracy, is no longer required.

Although voluminous studies have been conducted on understanding the properties of superconductors such as the critical temperature, current density, and magnetic field, the studies on the mechanical properties (hardness, elastic modulus, fracture toughness, ductility, etc.) are limited. In this study, we therefore aimed to examine the dynamical hardness measurements of polycrystalline superconductors in order to determine modulus and hardness values under different applied peak load and evaluate load dependency of the hardness and modulus.

2. Experimental

All of the samples were prepared by conventional solid-state reaction method. The powders of Y_2O_3, $BaCO_3$, and CuO were thoroughly mixed in appropriate amounts and calcined at 940 °C for 24 h. After calcination, the powders were mixed by a grinding machine for 4 h and then pressed into pellets of 13 mm diameter at 375 MPa. The pellets were sintered at 945 °C for 24 h and cooled down to room temperature at a cooling rate of 1 °C/min by flowing oxygen at temperatures between 700 and 250 °C. The sintered pellets were divided into three groups. The ZnO was added into the sintered pellets at the molar weight percentages of 0, 0.5, and 1% (0, 0.0024 and 0.0048 g). Detailed information for the samples characterization can be found elsewhere.[7] We use the sample labels Y_1, Y_2, and Y_3 to refer the samples with 0, 0.5 and 1% content of ZnO added to YBCO, respectively. Density of samples was measured by the Archimedes method using diethyphthalate as the immersion liquid. The densities of sintered Y_1, Y_2, and Y_3 pellets were 4.71, 5.34, and 5.93 g/cm^3, respectively.

Test specimen was obtained from machined surfaces. Damage on surface due to machinization was removed mechanically by grinding on 1000 and 1200 grit and then polishing on 6, 3, and 1 μm diamond lap wheels.

A Vickers indenter was used in a dynamic ultra microhardness tester (Shimadzu, DUH-W201S). All tests were performed under the same operating conditions. For an easier interpretation of the material behaviour at various depths, only the maximum load was changed at regular intervals; 0.49, 0.73, 0.98, and 1.22 N, where loading rate and dwell time were 0.013 N/s and 15 s at each peak load. In the depth-sensing hardness measurements, the indentation depth (h) and the load (P) were recorded by a computer. The raw data were then used to construct the load–displacement plots.

3. Theoretical background

Two mechanical properties, namely, elastic modulus E and microhardness H can be obtained with the load and penetration depth data. A typical load–penetration depth curve is shown in Fig. 1. During indenter loading, test material is subjected to both elastic and plastic deformation. The three

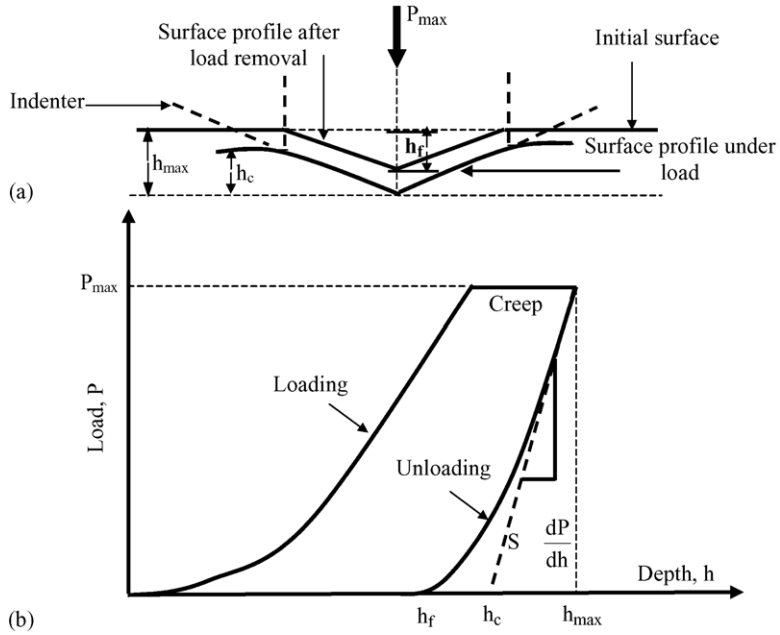

Fig. 1. Schematic plots of (a) cross-section of an indentation and (b) a typical load–displacement curve showing the values used in the Oliver and Pharr method.

key parameters needed to determine the hardness and modulus are the peak load (P_{max}), the contact area (A_c) and the initial unloading contact stiffness (S).

Similar to the conventional microhardness testing, the microindentation hardness is usually defined as the ratio of the peak indentation load, P_{max}, to the projected area of the hardness impression, A_c, i.e.

$$H = \frac{P_{max}}{A_c} = \frac{P_{max}}{26.43h_c^2} \qquad (A_c = 26.43h_c^2) \tag{1}$$

Different approaches for deducing the contact depth, h_c, from the resultant load displacement curve have been purposed and perhaps the most widely used one is that of Oliver and Pharr.[8] The Oliver and Pharr data analysis procedure begins by fitting unloading curve to and empirical power-law relation.

$$P = \alpha(h - h_f)^m \tag{2}$$

where P is the indentation load, h is the penetration depth, h_f is the final unloading depth and α and m are empirically determined fitting parameters. Using the initial part of the unloading curve, both stiffness and contact depth are determined by differentiating Eq. (2) at the maximum depth of penetration, $h = h_{max}$. Then, the stiffness of the contact is given by

$$S = \frac{dP}{dh} = \frac{2}{\sqrt{\pi}} E^* \sqrt{A_c} \tag{3}$$

where E^* is the reduced elastic modulus.

In this study, the Oliver and Pharr method was used to calculate the initial stiffness (S), contact depth (h_c) and hence reduced modulus (E^*) and hardness (HV).

4. Results and discussion

A series of indentations were made on the polycrystalline superconductors. The load–displacement curves shown in Figs. 2–4 (for Y_1: YBCO, Y_2: YBCO + 0.5% ZnO, and Y_3: YBCO + 1% ZnO, respectively) represent the applied load as a function of the displacement (elastic and plastic) of the indenter with respect to the initial position of the surface. It is apparent that the indentation depth of Y_2 (Fig. 3) and Y_3 (Fig. 4) samples for each applied peak load are lower than that of the Y_1 (Fig. 2), which implies the higher hardness for Y_2 and Y_3 samples.

Additionally, a typical contact depth (h_c) obtained from the analysis of the unloading curve is depicted as an inset plot in each figure (Figs. 2–4). The inset plots show the segment of unloading parts at 0.73 N for each specimen. Using the best fit values of the contact depth, h_c, HV numbers of the samples are calculated using Eq. (1). The results are plotted as a function of the peak load in Fig. 5. This figure clearly indicates that HV numbers decrease with increasing applied peak load. Since hardness is accepted as an inherent material property, it should not vary with indentation load and size. However, investigations [9–11] have confirmed that HV numbers of bulk materials were indentation size dependent especially at lower peak loads. Increase in hardness with decreasing applied peak load and hence indentation depth is called indentation size effect (ISE).[9–11] Fig. 6 exhibits this kind of behaviour. The figure was constructed experimentally using the data taken from the loading part of depth setting HV measurements at 0.73 N applied peak load for each sample.

The indentation size effect has been examined extensively for different kind of materials. Many attempts have been made to clarify the load dependence and to develop more or

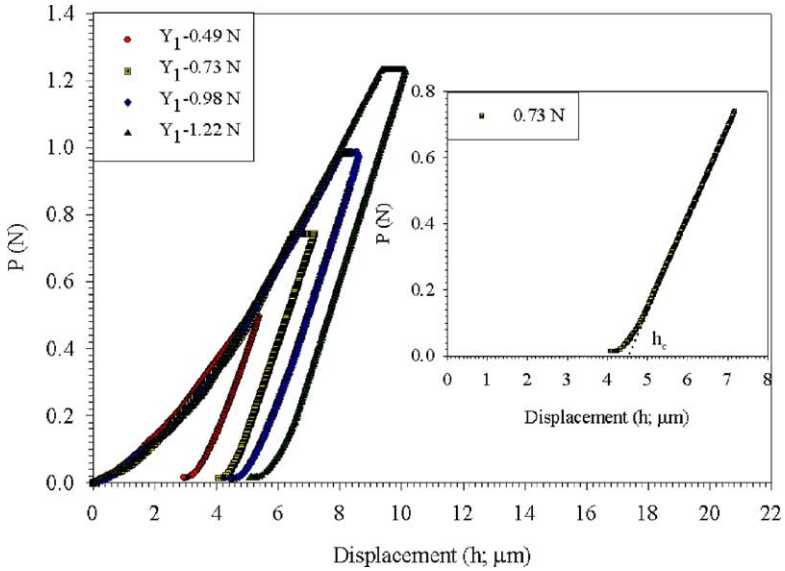

Fig. 2. A series of load–displacement plots at different peak loads for Y_1; YBCO sample. The inset depicts contact depth obtained from the analysis of the unloading curve at 0.73 N for the same sample.

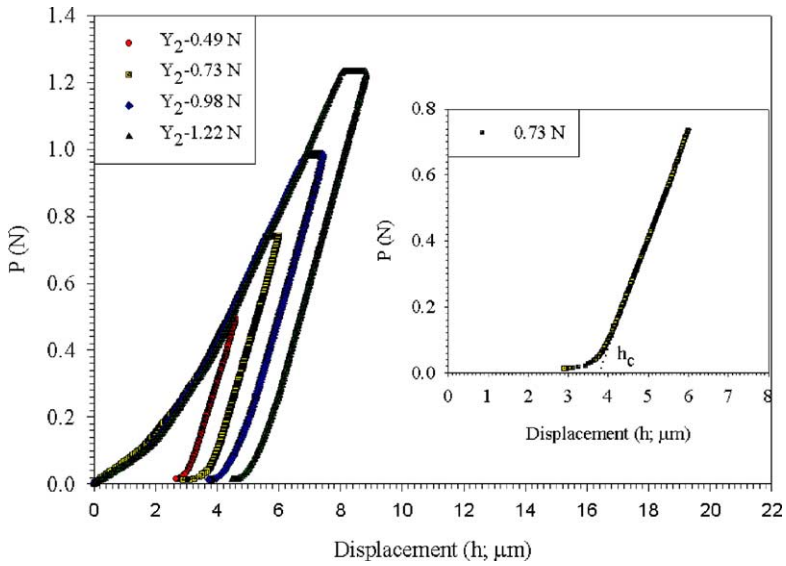

Fig. 3. A series of load–displacement plots at different peak loads for Y_2; YBCO + 0.5% ZnO sample. The inset depicts contact depth obtained from the analysis of the unloading curve at 0.73 N for the same sample.

less realistic models to interpret hardness tests.[12–17] The energy balance model, originally suggested by Fröhlich et al.,[18] is commonly used to explain ISE behaviour. According to this model, the indentation load, P, and the resultant indentation size, d, can be correlated with an empirical equation,

$$Pd = \alpha' d^2 + \beta' H_L d^3 \qquad \left(\beta' \frac{1}{k} = \frac{1}{1.8544}\right) \tag{4}$$

where α' and β' are constants and H_L is the true hardness or load independent hardness. Derivation and explanation of Eq. (4) were given in our earlier study.[17] Note that the indentation size, d, is proportional to the contact depth at the peak load, h_c based on the indenter geometry. Thus, an expression similar to Eq. (4) can be obtained for the depth-sensing microindentation test;

$$P_{max} h_c = \alpha(h_c^2) + \beta(H_L) h_c^3 \tag{5}$$

where α and β are constants. For a Vickers diamond tip, the constant β is given by the expression $\beta = (1/K) = 1/0.03784 = 26.43$, where K is a constant dependent only on the geometry of Vickers indenter.

Eq. (5) can also be interpreted from a different point of view. By dividing this equation by h_c^2, one gets

$$\frac{P_{max}}{h_c} = \alpha + \beta H_L h_c \tag{6}$$

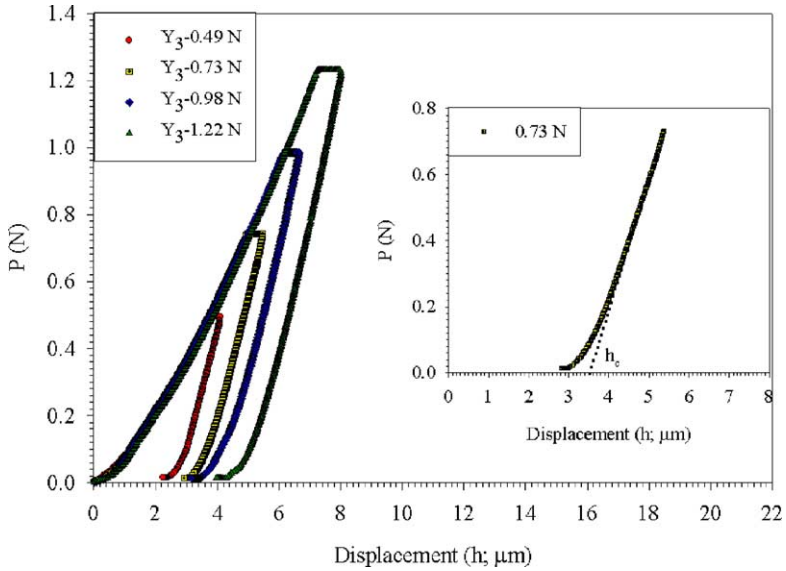

Fig. 4. A series of load–displacement plots at different peak loads for Y_3; YBCO + 1% ZnO sample. The inset depicts contact depth obtained from the analysis of the unloading curve at 0.73 N for the same sample.

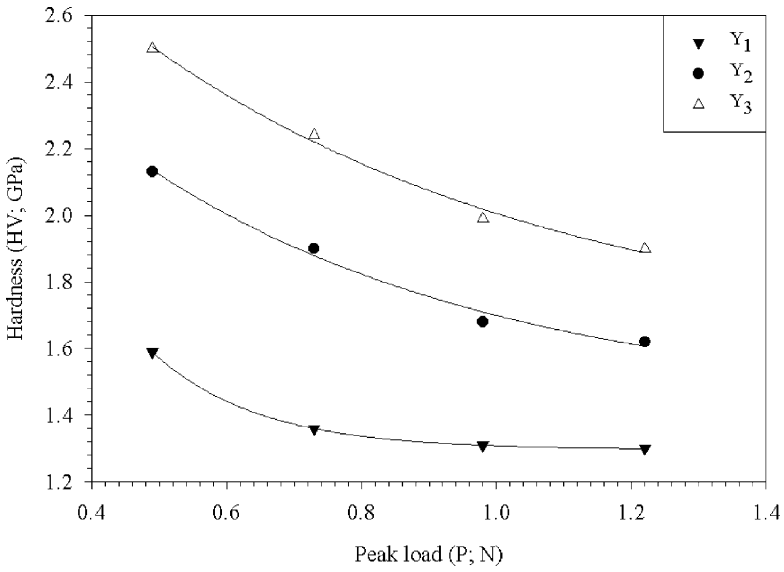

Fig. 5. Hardness variation with applied peak load.

which means that the load independent hardness is the slope of P/h versus h line. The existence linearity is shown in Fig. 7 constructed from the experimental data in the loading segment of the load–displacement curve at 0.73 N peak load for each specimen. If the deviation from the linearity for initial part of the plot is ignored, we can get a good linearity for each sample. Similar phenomenon was also observed in literature.[19]

On the other hand, it can be clearly seen from Fig. 5 that the hardness values are strongly dependent on peak load. Hence, the hardness value obtained from the slope of $P/h-h$ graph as seen in Fig. 7 for one peak load cannot be appropriate. Because, the displacement, h, used to construct the plot in Fig. 7 is not real contact depth and the displacement of the specimen surface at the perimeter of the contact.[19] We, therefore, think that the slope of $(P_{max}/h_c) - h_c$ graph constructed the using of real contact depths at different peak loads leads to more realistic results. As mentioned above, the h_c value in each peak load was calculated by using Oliver and Pharr method applied by making use of computer software that provided by Shimadzu, the company which supplied the dynamic ultra microhardness tester as well.

Fig. 8 shows such graphs constructed using the best fit values of the contact depths at different peak loads (0.49, 0.73, 0.98, and 1.22 N) for our Y_1, Y_2 and Y_3 samples. There are good linearities with correlation coefficients of 0.99, 0.98 and, 0.99 for Y_1, Y_2, and Y_3 specimens, respectively. The lines on such a plot will have slopes βH_L and

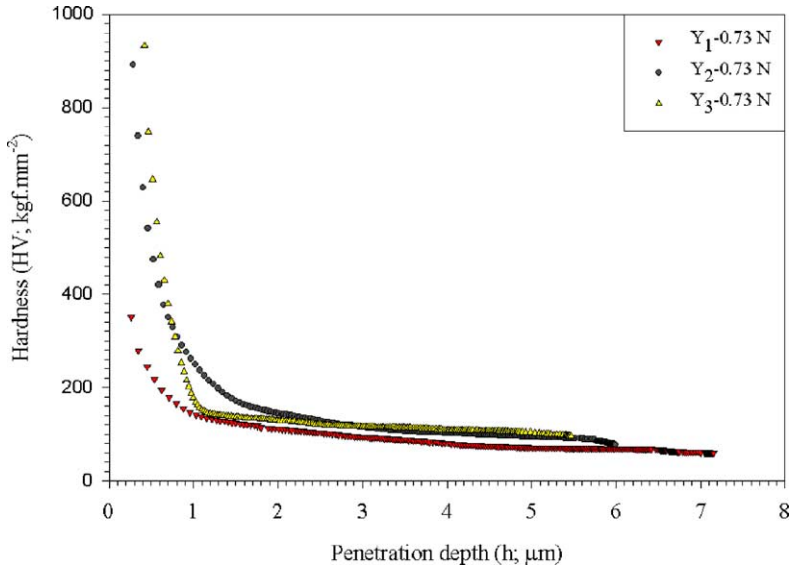

Fig. 6. Hardness variation with penetration depth.

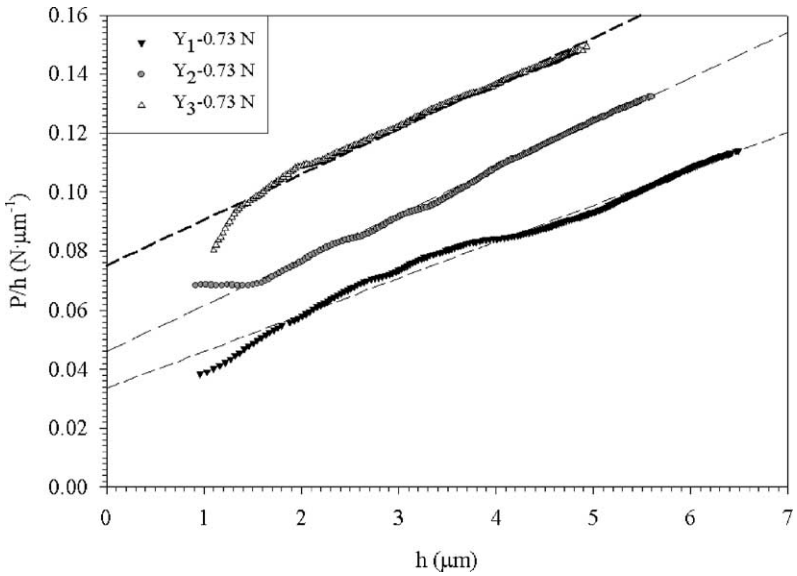

Fig. 7. The experimental data in the loading segments of the load displacement curves at 0.73 N peak load shown in Figs. 2–4 were re-plotted in a P/h vs. h scale.

y-intercepts of α for each specimen. So, it can be easily calculated the load independent hardness value (H_L) for each specimen.

On the other hand, reduced elastic modulus, E^*, is obtained from the analysis of the unloading curves using the Oliver and Pharr method as mentioned previously. By substituting A_c (Eq. (1)) into Eq. (3), one can easily get the following expression.

$$S = \frac{dP}{dh} = \frac{2}{\sqrt{\pi}} E^* \sqrt{26.43} h_c \quad (7)$$

Eq. (9) is the basic equation for determination of reduced elastic modulus by microindentation. The key quantities are the initial unloading contact stiffness, $S = dP/dh$ (i.e. the slope of the initial portion of the unloading curve) and the real contact depth, h_c in order to determine E^*.

Using the experimentally determined S and h_c, the reduced elastic modulus by microindentation was calculated and the results are shown in Fig. 9. It is clearly seen from the figure that the extracted reduced elastic modulus also exhibits a strong peak load dependency. Therefore, one can conclude that reduced elastic modulus cannot be extracted from the load–displacement curve resulting from only one peak load.

As can be seen from Eq. (7), there is a linear relationship between initial unloading stiffness, S, and the contact depth at peak load, h_c. Hence, the reduced elastic modulus can be obtained directly from the slope of the best fit lines for all

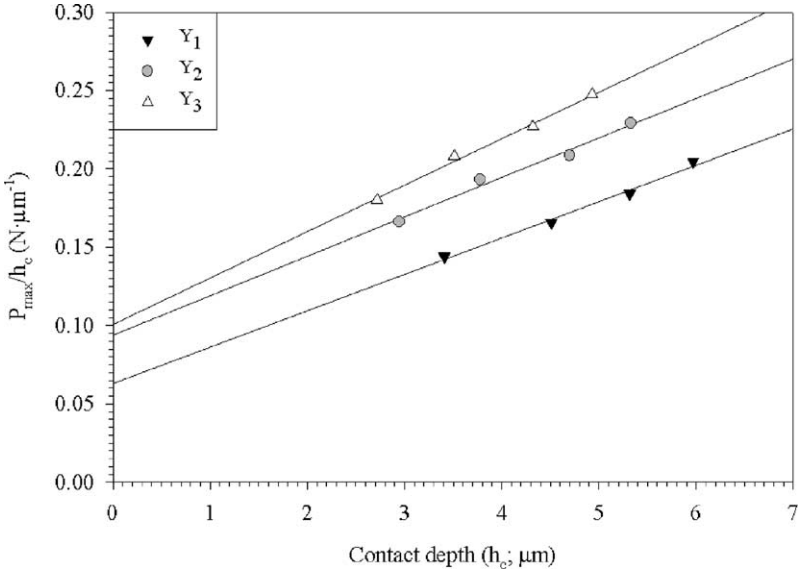

Fig. 8. P_{max}/h_c vs. h_c plots for each sample.

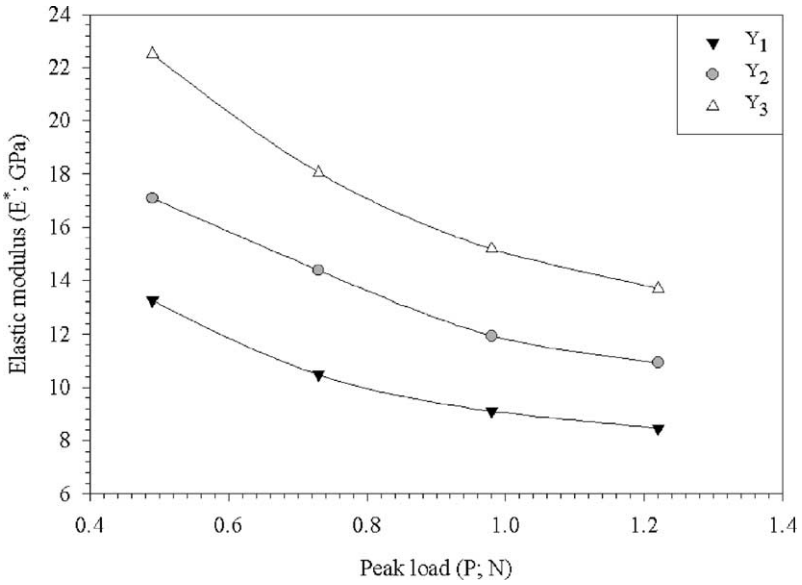

Fig. 9. The elastic modulus extracted from the analysis of the load displacement curves as a function of the peak loads for each sample.

specimens. In Fig. 10, the experimentally determined S is plotted as a function of the contact depth at peak load, h_c, Obviously, a good linearity exists between these two quantities for all specimens. The correlation coefficients obtained from the linear regression analysis are 0.98, 0.97, and 0.99 for Y_1, Y_2, and Y_3 samples, respectively.

The load independent hardness, H_L,values obtained from the slopes of the best fit lines in Fig. 8, the load independent reduced elastic modulus, $E_L{}^*$ determined by using similar way in Fig. 10 and experimentally determined two key parameters (S and h_c) are given in Table 1 as combined for each specimen. In general, the reduced elastic modulus increases with increasing hardness.[20] This simplest situation is also observed from the table for our samples.

On the other hand, the hardness and elastic modulus values from the present and previous investigations [7] are not in good agreement. Even, our previous reported hardness results for the same compositions do not show conformity with our present results. As an example, the highest hardness value is 2.50 GPa for the Y_3 sample with 0.49 N applied load while the corresponding value for the same composition at the same applied load is about 18 GPa. It is clearly seen that the microhardness value with 0.49 N applied load is very low compare with the previous result. The similar lover case also exists for other Y_1 and Y_2 samples. We believe that the lack of the conformity may arise from the difference in sample preparation method for microindentation experiment and measurement technique between our present

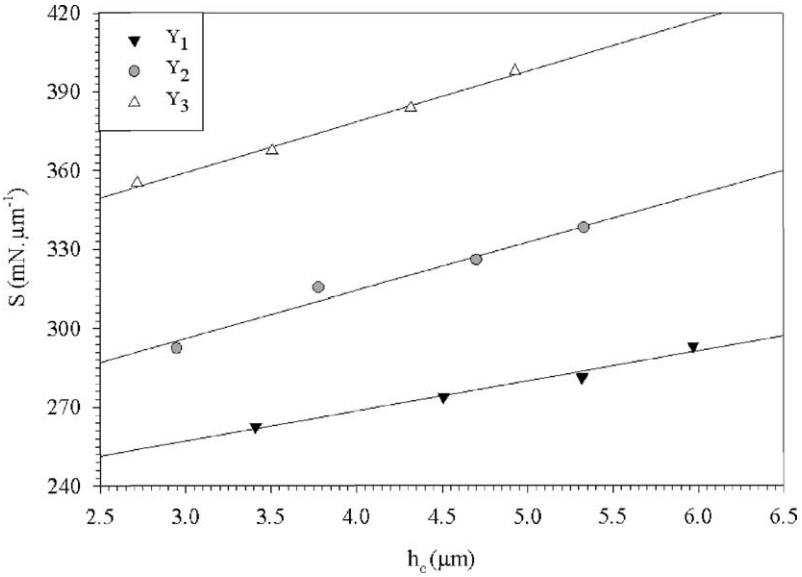

Fig. 10. Variation of the initial unloading stiffness with the contact depth at peak load for each sample.

Table 1
Results of microindentation analysis and density measurement for each sample

Sample	Peak load (N)	H_v (GPa)	H_L (GPa)	E^* (GPa)	$E_L{}^*$ (GPa)	h_c (μm)	S (mN/μm)	d (g/cm^3)
Y_1	0.49	1.59	0.88	13.27	1.98	3.41	262.59	4.71
	0.73	1.36		10.47		4.51	273.93	
	0.98	1.31		9.11		5.32	281.24	
	1.22	1.30		8.46		5.97	293.15	
Y_2	0.49	2.13	0.95	17.09	3.13	2.95	292.45	5.34
	0.73	1.93		14.38		3.78	315.46	
	0.98	1.68		11.94		4.70	325.86	
	1.22	1.62		10.92		5.33	337.90	
Y_3	0.49	2.50	1.12	22.51	3.33	2.72	355.13	5.93
	0.73	2.24		18.05		3.51	367.56	
	0.98	1.99		15.19		4.32	380.63	
	1.22	1.90		13.70		4.93	391.90	

and previous studies. As a matter of the fact that the samples in the previous study were not exposed to any grinding and polishing treatment, although, the samples in the present work were polished before microindentation experiment.

Another interesting point is that, there is a good agreement between load independent hardness values of the present and previous results for the same samples contrary to the lack of conformity, mentioned above, hardness values with one applied load. Therefore, a load independent hardness value (H_L) becomes important to make a meaningful comparison among the literature results.

Accordingly, the elastic modulus values of the present work are also lower than the reported literature results.[21] In literature, several measurements of the Young's modulus for similar HTS samples have resulted in values falling within the range $E = 40$–370 GPa. We think that the lower elastic modulus values as similar the hardness results in the present study may arise from the polishing treatment before the dynamic microindentation. It is however obviously seen from the literature that the reported elastic modulus values for comparable YBCO materials show a significant variation. As well, it was reported a very low elastic constant value (about 5 GPa) for a YBCO material.[22] These very different values may probably arise from several factors (e.g. sample production method, microstructural differences such as the ratio and the distribution of minority phase (2 1 1), porosity, bad contact between grains, test conditions and so on). Additionally, one should point out that the elastic modulus of YBCO samples in the present study shows strong dependency on applied load. Hence, it is useful to compare the load independent Young's modulus among the literature results. In this study, we therefore focused on the load independent hardness and elastic modulus values.

In addition, the hardness can be primarily related with the porosity. The increase in bulk density is indication of decrease in porosity which implies hardness increasing. This relation between hardness and density was reported by some other researchers.[23,24] In order to estimate the effect of ZnO addition on porosity of the samples, we measured the density of the samples and results were given in Table 1. When the results are examined comparatively, it is clearly seen that all measured and calculated characteristic parameters of the samples (i.e. density, reduced elastic modulus and hardness) increase with increasing ZnO content.

5. Conclusion remarks

A microindentation method has been used to measure the mechanical properties of polycrystalline superconductor samples. The microhardness and reduced elastic modulus of polycrystalline samples were deduced by analyzing the unloading segments of the load–displacement curves using the widely adopted Oliver and Pharr method. Additionally, we examined the relation between hardness and density results of the samples and the following results were obtained.

1. Vickers microhardness values of the samples was obviously load dependent.
2. The variation of microhardness, with increasing peak load range from 1.59 GPa at 0.49 N to 1.30 GPa at 1.22 N for Y_1. The correspondence values at the same peak loads range from 2.13 to 1.62 GPa and 2.50 to 1.90 GPa for Y_2 and Y_3, respectively.
3. The peak load dependence of the hardness shows a typical ISE behaviour. Application of the energy-balance model can be used to determine the load independent hardness values. The values obtained from the (P/h_c) versus h_c plots are 0.88, 0.95, and 1.22 GPa for Y_1, Y_2, and Y_3, respectively.
4. The hardness values and densities of the samples increase with increasing ZnO content. The increase in bulk density is indication of decrease in porosity.
5. The load independent reduced elastic modulus, $E_L{}^*$, extracted directly using the conventional stiffness equation, Eq. (7), also exhibits a peak load dependency. Therefore, a reasonable peak load independent modulus can be determined directly from the slope of the best-fit

straight line between initial unloading stiffness, S, and the contact depth at peak load, h_c. The obtained values of $E_L{}^*$ are 1.98, 3.13, and 3.33 GPa for Y_1, Y_2, and Y_3, respectively.

Acknowledgements

We are indebted to the Turkish State Planning Organisation (DPT) for its financial support (Project No.: 2003K120510) in our acquiring the dynamic microhardness tester equipment. This work was also supported by the Research Fund of Karadeniz Technical University, Trabzon, Turkey, under the grant contract no.: 2002.111.1.5.

References

1. Mott, B. W., *Micro-indentation Hardness Testing*. Butterworths, London, 1956, p. 206.
2. Giannakopoulos, A. E. and Suresh, S., *Scripta Materialia* 1999, **40**(10), 1191–1198.
3. Elmustafa, A. A. and Stone, D. S., *Acta Materialia* 2002, **50**, 3641–3650.
4. Atar, E., Çimenoğlu, H. and Kayalı, E. S., *Surface Coat. Technol.* 2003, **162**, 167–173.
5. Gogotsi, Y., Miletich, T., Gardner, M. and Rosenberg, M., *Rev. Scientific Instrum.* 1999, **70**(12), 4612–4617.
6. Zhu, W. and Bartos, P. J. M., *Cement Concentrate Res.* 2000, **30**, 1299–1304.
7. Kölemen, U., Çelebi, S., Karal, H., Öztürk, A., Nezir, S. and Görür, O., *Phys. Stat. Sol. (b)* 2004, **241**(2), 274–283.
8. Oliver, W. C. and Pharr, G. M., *J. Mater. Res.* 1992, **7**(6), 1564–1583.
9. Krell, A. and Schadlich, S., *Int. J. Refractory Metals Hard Mater.* 2001, **19**, 237–243.
10. Lal, B., Bamzai, K. K. and Kotru, P. N., *Mater. Chem. Phys.* 2002, **78**, 202–207.
11. Louro, C., Cavaleiro, A., Dub, S., Smid, P., Musil, J. and Vlcek, J., *Surface Coat. Technol*. 2002, **161**, 111–119.
12. Kotru, P. N., Raina, K. K., Kachroo, S. K. and Wanklyn, B. M., *J. Mater. Sci*. 1984, **19**, 2582–2592.
13. Gong, J., Wu, J., Guan, Z. and Miao, H., *Mater. Lett.* 1999, **38**, 197–201.
14. Gong, J., Zhao, Z., Guan, Z. and Miao, H., *J. Eur. Ceram. Soc.* 2000, **20**, 1895–1900.
15. Sangwall, K., Surowska, B. and Blaziak, P., *Mater. Chem. Phys.* 2002, **77**, 511–520.
16. Sangwall, K., Surowska, B. and Blaziak, P., *Mater. Chem. Phys.* 2003, **80**, 428–437.
17. Uzun, O., Karaaslan, T. and Keskin, M., *J. Alloys Compounds* 2003, **358**, 104–111.
18. Fröhlich, I., Graw, F. P. and Wrellmann, W., *Phys. Status Sol.* 1977, **42**, 78–89.
19. Gong, J., Miao, H., Peng, Z. and Qi, L., *Mater. Sci. Eng. A* 2003, **354**, 140–145.
20. Musil, J., Kunc, F., Zeman, H. and Polakova, H., *Surface Coat. Technol.* 2002, **154**, 304–313.
21. Johansen, T. H., *Supercond. Sci. Technol*. 2000, **13**, R121–R137.
22. Low, I. M., Skala, R. D. and Mohazzab, G., *J. Mater. Sci. Lett*. 1994, **13**, 1340–1342.
23. Harris, L. B. and Nyung, F. K., *J. Mater. Sci. Lett.* 1988, **7**, 801–803.
24. Lubenets, S. V., Natsik, V. D., Fomenko, L. S., Kaufmann, H. J. and Bobrov, V. S., *Low Temp. Phys.* 1997, **23**, 678–683.